IEEE Access
Multidisciplinary | Rapid Review | Open Access Journal

Received November 4, 2019, accepted November 21, 2019, date of publication November 25, 2019,
date of current version December 11, 2019.

Digital Object Identifier 10.1109/ACCESS.2019.2955750

Optimum LoRaWAN Configuration Under Wi-SUN Interference

ARLIONES HOELLER[1,2,3], (Member, IEEE),
RICHARD DEMO SOUZA[2], (Senior Member, IEEE),
HIRLEY ALVES[3], (Member, IEEE),
ONEL L. ALCARAZ LÓPEZ[3], (Member, IEEE),
SAMUEL MONTEJO-SÁNCHEZ[4], (Member, IEEE),
AND MARCELO EDUARDO PELLENZ[5]

[1]Department of Telecommunications, Federal Institute for Education, Science, and Technology of Santa Catarina, São José 88103-310, Brazil
[2]Department of Electrical and Electronics Engineering, Federal University of Santa Catarina, Florianópolis 88040-900, Brazil
[3]Centre for Wireless Communications, University of Oulu, 90014 Oulu, Finland
[4]Programa Institucional de Fomento a la Investigación, Desarrollo e Innovación (PIDi), Universidad Tecnológica Metropolitana, Santiago 8940577, Chile
[5]Informatics Graduate Program, Pontifical Catholic University of Paraná, Curitiba 80215-901, Brazil

Corresponding author: Arliones Hoeller (arliones.hoeller@ifsc.edu.br)

This work was supported in part by the Brazilian National Council for Scientific and Technological Development (CNPq); in part by Brazilian Print CAPES-UFSC "Project Automation 4.0"; in part by INESC P&D Brazil Project F-LOCO, under Grant Energisa/ANEEL PD-00405-1804/2018; in part by the Academy of Finland (Aka) 6Genesis Flagship, under Grant 318927; in part by Project EE-IoT, under Grant 319008; in part by Aka Prof, under Grant 307492; and in part by the FONDECYT Postdoctoral Chile, under Grant 3170021.

ABSTRACT Smart Utility Networks (SUN) rely on the Wireless-SUN (Wi-SUN) specification for years. Recently practitioners and researchers have considered Low-Power Wide-Area Networks (LPWAN) like LoRaWAN for SUN applications. With distinct technologies deployed in the same area and sharing unlicensed bands, one can expect these networks to interfere with one another. This paper builds over a LoRaWAN model to optimize network parameters while accounting for inter-technology interference. Our analytic model accounts for the interference LoRaWAN receives from IEEE 802.15.4g networks, which forms the bottom layers of Wi-SUN systems. We derive closed-form equations for the expected reliability of LoRaWAN in such scenarios. We set the model parameters with data from real measurements of the interplay among the technologies. Finally, we propose two optimization algorithms to determine the best LoRaWAN configurations, given a targeted minimum reliability level. The algorithms maximize either communication range or the number of users given constraints on the minimum number of users, minimum communication range, and minimum reliability. We validate the models and algorithms through numerical analysis and simulations. The proposed methods are useful tools for planning interference-limited networks with requirements of minimum reliability.

INDEX TERMS Internet-of-things, low-power wide-area networks, communication interference.

I. INTRODUCTION

Smart Utility Networks (SUN) are key enablers of Smart Cities [1]. In such environments, the Internet-of-Things (IoT) plays a paramount role in connecting massive numbers of devices like smart meters, smart light bulbs, and smart appliances. Besides the existence of several potential network technologies, *e.g.*, LoRaWAN, SigFox and Wi-SUN , the reliable and efficient connection of massive numbers of devices is still a challenge [2].

The associate editor coordinating the review of this manuscript and approving it for publication was Giacomo Verticale.

Industry backs two initiatives: LoRa Alliance and Wi-SUN Alliance. LoRa Alliance – supported by Semtech, IBM, Cisco, Orange, among others – maintains the LoRaWAN specification [3]. LoRaWAN is a Low-Power Wide-Area Network (LPWAN) technology operating in the sub-GHz ISM band, using chirp spread-spectrum modulation, allowing increased signal robustness and range at low power consumption and low data rates [1]. LoRaWAN uses the LoRa physical layer (PHY) designed by Semtech and specifies the upper layer protocols to enable IoT deployments. Wi-SUN Alliance – supported by Cisco, Analog Devices, Toshiba, and others – maintains the Wi-SUN

specification [4], [5]. Wi-SUN is a Field Area Network (FAN) technology built upon the physical and link layers defined by the IEEE 802.15.4g standard. IEEE 802.15.4g operates in different ISM bands, including the same sub-GHz bands used by LoRaWAN, where it employs a Gaussian Frequency Shift Keying (GFSK) modulation over narrow-band channels. Wi-SUN also defines network- and application-level services and profiles for different utility applications (e.g., energy, gas, water).

While utility service providers modernize their systems to use smart meters, deployments can use different communication technologies in the same geographical region, thus raising the question of how inter-technology interference affects network scalability. Coordination among transmissions in different technologies is unfeasible at the network or lower layers, so it is essential to understand the impact of external interference through use cases, theoretical analysis, and design strategies [6]. To achieve a realistic model, one should take into account that LPWAN devices in the ISM radio band are subject to interference generated by other networks sharing the same part of the spectrum. For instance, different authors report the analysis of the interaction of LoRa with other technologies considering IEEE 802.15.4g [7], SigFox [8], [9], and IEEE 802.11ah [9]. The results in those papers suggest that LoRa susceptibility to interference arriving from other technologies depends not only on the activity on those interfering networks but also on the configuration of the LoRa signal, mainly the spreading factor (SF). In this paper, we consider LoRaWAN as our target technology and model its performance in the presence of IEEE 802.15.4g interference sources in the sub-GHz ISM band (e.g., around 868 MHz in Europe and 915 MHz in USA/Brazil). Please note that the restriction of the model to IEEE 802.15.4g interference comes without loss of generality since one can extend it to other network technologies provided that appropriate isolation thresholds between the technologies are available.

In our work, we evolve from previous developments in [10] and [11] to approach the problem from an analytic perspective. We derive two optimization algorithms that explore the configuration space of LoRaWAN in the presence of internal and external interference. The algorithms are network planning tools for massive IoT applications, guiding the trading-off between reliability, the number of users, and coverage area/range. We validate our analytic findings with simulations configured according to experimental results on the interplay of these networks published in [7]. We do not consider latency in this paper because our methods do not impact latency. A good third-party work that analyzes the latency of Class A LoRaWAN is [12].

The contributions of this work include a closed-form expression for the inter-SF LoRaWAN interference model of [11]; the extension of the analytic models of [10] and [11] to consider external interference; the performance analysis of LoRaWAN considering the experimental results on inter-technology interference from [7]; and two algorithms to optimize LoRaWAN configuration, either in terms of network load or communication range, under reliability constraints.

The remaining of this paper is organized as follows. Section II summarizes related work, and Section III briefly introduces the characteristics of LoRaWAN and IEEE 802.15.4g . Section IV introduces the proposed models. Section V presents the proposed algorithms. Section VI evaluates the models and algorithms. Section VII concludes the paper.

II. RELATED WORK

Georgiou and Raza [13] propose an analytic model of LoRaWAN, which considers both disconnection and collision probabilities in Rayleigh fading channels. They show that LoRaWAN is sensitive to node density because it affects collision probability. In [10], we extend the work of [13] to exploit message replications and multiple receive antennas at the gateway. We show that message replication is an interesting option for low-density networks, while the performance gains from spatial diversity are significant in all cases. Mahmood *et al.* [11], as well as we [10] and Georgiou and Raza [13], use stochastic geometry and Poisson Point Processes (PPP) to derive analytic models of the LoRaWAN coverage probability. Contrasting with [13] and [10], the work in [11] considers the effect of interference from the imperfect orthogonality of LoRa signals with different SF.

Orfanidis *et al.* [7] report an experimental evaluation of the interference between IEEE 802.15.4g and LoRa by measuring the packet error ratio in different SINR scenarios inside an anechoic chamber. The measurements consider a single IEEE 802.15.4g interferer over one LoRa link. Their results show that lower SFs are more susceptible to interference. Although these measurements show interesting results, it is important to note that they consider a limited number of nodes, thus making it hard to extrapolate the conclusions. To the best of our knowledge, no other work has studied the susceptibility of LoRa to external IEEE 802.15.4g interference, and there is none published work that investigates this relationship in a network-scale scenario with several active links in both IEEE 802.15.4g and LoRaWAN .

III. LPWAN NETWORKS

LPWAN technologies employ low-power communication mechanisms to enable the connection of thousands of IoT devices. Most technologies work in sub-GHz frequencies and feature link budgets of 150 ± 10 dB, implementing robust communication channels with low energy consumption reaching distances in the order of kilometers [1]. For reducing complexity and energy consumption, LPWANs use MAC protocols that may decrease channel usage efficiency. For instance, the unslotted ALOHA MAC in LoRaWAN presents high collision probability with large numbers of users [14].

A. LoRaWAN

LoRa is a proprietary sub-GHz chirp spread spectrum modulation technique optimized for long-range

TABLE 1. LoRa Uplink characteristics for 9-byte packets, $B = 125$ kHz, CRC and header mode enabled, and FEC rate $\frac{4}{5}$ for the SX1272 transceiver [16].

SF i	ToA t_i (ms)	Bitrate Rb_i (kbps)	Receiver Sensitivity $\mathcal{S}_i$ (dBm)	SNR threshold ψ_i (dB)
7	41.22	5.47	-123	-6
8	72.19	3.12	-126	-9
9	144.38	1.76	-129	-12
10	247.81	0.98	-132	-15
11	495.62	0.54	-134.5	-17.5
12	991.23	0.29	-137	-20

low-power applications at low data rates [3]. LoRa modulation depends, basically, on three parameters [15]: bandwidth (B), usually set to 125 kHz or 250 kHz for uplink and 500 kHz for downlink; SF, which assumes values from 7 up to 12; and the forward error correction (FEC) rate, varying from $\frac{4}{8}$ to $\frac{4}{5}$. The parameters allow computing packet Time-on-Air (ToA), receiver sensitivity, and required signal-to-noise ratio (SNR) for successful detection in the absence of interference, which Table 1 presents for a given packet configuration. Note that ToA grows exponentially with SF, reducing the data rate and decreasing receiver sensitivity, improving coverage.

The LoRa PHY is agnostic of higher layers. LoRaWAN is the most widely used protocol stack for LoRa networks. It implements a star topology where *end-devices* (nodes) connect through a single-hop to one or more *gateways*, which in turn connect to a *network server* via an IP network. Moreover, a LoRa gateway can process up to nine channels in parallel, combining different sub-bands and SF [1]. LoRa features the capture effect, making it possible to recover a LoRa signal when two or more signals are received simultaneously, in the same frequency and SF, provided that the desired signal is at least 1 dB above interference [17].

B. IEEE 802.15.4g

IEEE 802.15.4g is an amendment to the IEEE 802.15.4 standard focusing on Smart Utility Networks (SUN) that plays an important role in the smart grid [18]. The standard specifies several modes operating in different bands, including the Sub-GHz ISM bands used by LoRaWAN . Multi-Rate FSK (MR-FSK), with 2-FSK or 4-FSK, is the predominant modulation version in SUN applications due to its communication range [19]. In this configuration, the transceiver combines FSK modulation with Frequency Hopping Spread Spectrum (FHSS) to increase robustness [20]. Data rate varies from 2.4 to 200 kbps, depending on region and frequency band.

The mandatory configuration for all regions is 2-FSK operating at 50 kbps, which implies a channel spacing of 200 kHz. Transmit power depends on regional regulations, but must be at least −3dBm [5]. Most configurations use 14dBm transmit power and 1% duty cycle [21]. IEEE 802.15.4g also extends the MAC mechanisms defined by the IEEE 802.15.4e amendment [22] to make extensive use of low-energy modes. IEEE 802.15.4g networks are expected to form multi-hop, mesh networks. Before sending data, the MAC performs either carrier sense or a simplified version of channel monitoring named Coordinated Sampled Listening (CSL) [23].

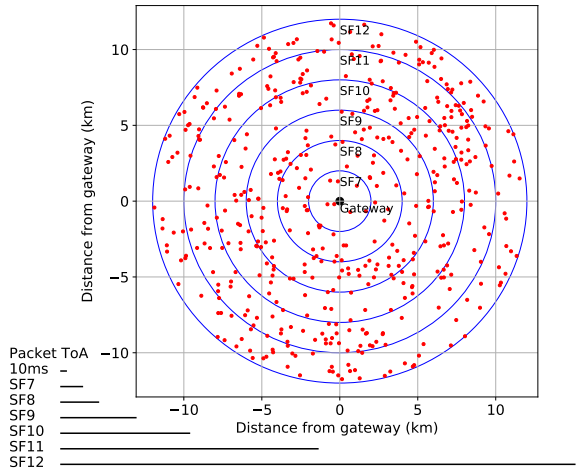

FIGURE 1. $\bar{N} = 500$ nodes uniformly distributed in a circular area of radius $R = 12000$ m around the gateway and with increasing SF every 2000 m. The ToA, as in Table 1, is illustrated in the lower-left corner.

IV. SYSTEM MODEL

Following the developments in [10] and [11], we use a set of Poisson Point Processes (PPP) [24]. Our model considers nodes deployed uniformly in a circular region around a gateway. Figure 1 illustrates a *possible* setup where SF increases according to the distance from the gateway. The figure, as in previous related work, uses the sub-optimal fixed-width SF rings, a problem we address in Section V. The vector $L = [l_0, \ldots, l_6]$, $l_0 = 0$, defines the limits of each SF ring. Note that $R = l_6$ is the maximum network communication range, *i.e.*, the coverage radius. LoRaWAN devices transmit in the uplink at random using the ALOHA protocol and transmit once in a given period T. Considering that all nodes run the same application, the network usage is different for each SF because of different data rates (see ToA in Table 1). Figure 1 also shows the ToA difference graphically. Hence, we model the transmission probability of LoRaWAN devices as a vector $p = [p_1, \ldots, p_6]$, $p_i \in (0, 1]\ \forall i \in \{1, \ldots, 6\}$, and $p_i = \frac{t_i}{T}$, where t_i is the ToA for SF of ring i. Note that, for the sake of simplicity, we define the set $S = \{1, \ldots, 6\}$ to denote the SF rings and that each ring uses a respective SF in $\{7, \ldots, 12\}$.

Each LoRaWAN SF ring constitutes a separated PPP, denoted Φ_i, $i \in S$, making it possible to attribute different densities to each SF. Φ_i has density $\alpha_i = p_i\rho_i$ in its area $V_i = \pi(l_i^2 - l_{i-1}^2)$, where l_{i-1} and l_i are, respectively, the inner and outer radii of SF ring i (from L), and ρ_i is the spatial density of nodes in V_i. The average number of nodes in Φ_i is $\bar{N}_i = \rho_i V_i$. The average number of nodes in the LoRaWAN network is $\bar{N} = \sum_{i \in S} \rho_i V_i$. For instance, take the ring $i = 2$ in Figure 1, defined by two circles of radii $l_1 = 2$km and $l_2 = 4$km. Nodes in this ring use SF_8. The ring area is $V_2 = \pi(l_2^2 - l_1^2) = 37.7\text{km}^2$. If there are,

on average, $\bar{N}_2 = V_2\rho_2 = 100$ nodes in this ring, then its spatial density is $\rho_2 = \frac{\bar{N}_2}{V_2} = 2.65$ nodes/km^2. Finally, if nodes transmit probability is 1% ($p_2 = 0.01$), the intensity of Φ_2 is $\alpha_2 = p_2\rho_2 = 0.0265$.

In addition to LoRaWAN, we consider an external IEEE 802.15.4g network operating in the same ISM bands and geographic region. Users of that network are spread across the LoRaWAN area. IEEE 802.15.4g transceivers in ISM sub-GHz bands employ bandwidth and transmit power configurations similar to LoRaWAN . So, we model the IEEE 802.15.4g network as an additional PPP where nodes transmit with probability $p_z \in (0, 1]$ in area $V_z = \pi R_z^2$, where $R_z \geq R$. The PPP Φ_z has density $\alpha_z = p_z\rho_z$, where ρ_z is the spatial density of nodes in V_z. The average number of nodes in Φ_z is $\bar{N}_z = \rho_z V_z$.

In our analysis, d_k is the Euclidean distance between the k-th node and the gateway, and d_1 denotes the distance of the node of interest. All nodes use the same transmit power $\mathcal{P}_t$ to send signal s_k, while both path loss and Rayleigh fading affect the received signals of LoRaWAN and IEEE 802.15.4g . Path loss follows $g(d_k) = \left(\frac{\lambda}{4\pi d_k}\right)^\eta$, with wavelength λ, path loss exponent $\eta \geq 2$, while k represents a device in either network. Finally, h_k denotes the Rayleigh fading. Therefore, a LoRaWAN signal r_1 received at the gateway is the sum of the attenuated transmitted signal s_1, interference, and noise,

$$r_1 = g(d_1)h_1\, s_1 + \mathcal{I}_L + \mathcal{I}_Z + n, \tag{1}$$

where

$$\mathcal{I}_L = \sum_{i\in S}\sum_{k\in\Phi_i} g(d_k)h_k s_k \tag{2}$$

accounts for intra-network interference, considering both co-SF and inter-SF interference by summing all other received signals from all SFs, and

$$\mathcal{I}_Z = \sum_{k\in\Phi_z} g(d_k)h_k s_k \tag{3}$$

models external interference arising, in our case, from all active nodes in the IEEE 802.15.4g network. Finally, n is the additive white Gaussian noise (AWGN) with zero mean and variance $\mathcal{N} = -174 + F + 10\log_{10}(B)$ dBm, where $F = 6$dB is the receiver noise figure and $B = 125$kHz is the LoRa channel bandwidth. The remainder of this section uses this model to derive a reliability model of LoRaWAN .

A. COVERAGE PROBABILITY

The *coverage probability* is the probability that the selected node is in coverage (not in outage), *i.e.*, it can successfully communicate in the presence of noise, internal interference, and external interference. The coverage probability of the desired node located d_1 meters from the gateway is thus

$$C_1(d_1) = H_1(d_1)Q_1(d_1)Z_1(d_1), \tag{4}$$

where H_1, Q_1, and Z_1 are described in the following sections and denote the success probability with regards to, respectively, noise, internal interference, and external interference.

B. OUTAGE CONDITION 1: DISCONNECTION

Following [10], we consider the disconnection probability, which depends on the communication distance. A node is *not* connected to the gateway if the SNR of the received signal is below the threshold that allows successful detection in the absence of interference. Receiver sensitivity is different for each SF, what results in different SNR reception thresholds defined in

$$\Psi_{[dB]} = \begin{matrix} SF_7 & SF_8 & SF_9 & SF_{10} & SF_{11} & SF_{12} \end{matrix}$$
$$\begin{bmatrix} -6 & -9 & -12 & -15 & -17.5 & -20 \end{bmatrix},$$

where Ψ is the SNR threshold vector, and ψ_i denotes the i-th element of Ψ, *i.e.*, the SNR threshold for SF ring i. Then, we model the *connection probability* as

$$H_1(d_1) = \mathbb{P}[\text{SNR} \geq \psi_i | d_1]. \tag{5}$$

Since we assume Rayleigh fading, the instantaneous SNR is exponentially distributed [25], and therefore

$$H_1(d_1) = \mathbb{P}\left[\frac{\mathcal{P}_t|h_1|^2\, g(d_1)}{\mathcal{N}} \geq \psi_i\right] = \exp\left(-\frac{\mathcal{N}\psi_i}{\mathcal{P}_t g(d_1)}\right). \tag{6}$$

C. OUTAGE CONDITION 2: INTRA-NETWORK INTERFERENCE

Intra-network interference arises from the activity of other devices in the same network. We follow [11] to model both co-SF and inter-SF interference. To recover a packet, the signal-to-interference ratio (SIR) at the gateway must be above a given threshold. The transceiver manufacturer informs that SFs are orthogonal and that the co-SF SIR threshold is +6dB [16]. Goursaud and Gorce [26] propose theoretical SIR thresholds that match Semtech co-SF value but show that different SFs are not entirely orthogonal. However, Croce *et al.* [17] showed, experimentally, that the SIR thresholds for Semtech SX1272 LoRa transceiver are lower with regards to co-SF interference ($\approx$ +1dB) but significantly higher with respect to (w.r.t.) inter-SF interference. In this paper, we assume the experimental SIR thresholds of [17]

$$\Delta_{[dB]} = \begin{matrix} & \text{SF}_7 & \text{SF}_8 & \text{SF}_9 & \text{SF}_{10} & \text{SF}_{11} & \text{SF}_{12} \end{matrix}$$
$$\begin{matrix} \text{SF}_7 \\ \text{SF}_8 \\ \text{SF}_9 \\ \text{SF}_{10} \\ \text{SF}_{11} \\ \text{SF}_{12} \end{matrix}\begin{bmatrix} +1 & -8 & -9 & -9 & -9 & -9 \\ -11 & +1 & -11 & -12 & -13 & -13 \\ -15 & -13 & +1 & -13 & -14 & -15 \\ -19 & -18 & -17 & +1 & -17 & -18 \\ -22 & -22 & -21 & -20 & +1 & -20 \\ -25 & -25 & -25 & -24 & -23 & +1 \end{bmatrix},$$

where Δ is the SIR threshold matrix, and $\delta_{i,j}$ denotes the element of Δ at the i-th line and j-th column, *i.e.*, the SIR threshold for the desired signal using SF_i and interference using SF_j. Note that $i = j$ relates to the co-SF SIR while $i \neq j$ relates to inter-SF SIR. If one takes the SF_7 column as an example, it shows how SF_7 interference affects the LoRa signals. Desired signals using higher SF are more robust to inter-SF interference, allowing for the decoding of LoRa packets even if the interference power is much higher than the signal (*e.g.*, 25dB higher if the signal uses SF_{12}).

Following this rationale, we first use the formulations in [11] to analyze the success probability considering the interference from only one different SF_j. Let

$$\mathrm{SIR}_j = \frac{|h_1|^2\, g(d_1)\mathcal{P}_t}{\mathcal{I}_j}, \tag{7}$$

where the interference received from nodes using SF_j is

$$\mathcal{I}_j = \sum_{k\in\Phi_j} |h_k|^2\, g(d_k)\mathcal{P}_t. \tag{8}$$

Since the desired node at d_1 uses SF_i, the success probability is

$$\begin{aligned} P_{\mathrm{SIR}_j}(d_1, j) &= \mathbb{P}[\mathrm{SIR}_j \geq \delta_{i,j}] \\ &= \mathbb{E}_{\mathcal{I}_j}\left[\mathbb{P}\left[|h_1|^2 \geq \frac{\mathcal{I}_j\delta_{i,j}}{g(d_1)\mathcal{P}_t}\right]\right]. \end{aligned}$$

Since $|h_1|^2 \sim \exp(1)$,

$$P_{\mathrm{SIR}_j}(d_1, j) = \mathbb{E}_{\mathcal{I}_j}\left[\exp\left(-\frac{\mathcal{I}_j\delta_{i,j}}{g(d_1)\mathcal{P}_t}\right)\right]. \tag{9}$$

Note that (9) has the form of the Laplace Transform w.r.t. $\mathcal{I}_j$, where $\mathcal{L}_{\mathcal{I}_j}(s) = \mathbb{E}_{\mathcal{I}_j}[\exp(-s\mathcal{I}_j)]$, $s = \frac{\delta_{i,j}}{g(d_1)\mathcal{P}_t}$. Thus, using (8) and applying the property of the sum of exponents,

$$P_{\mathrm{SIR}_j}(d_1, j) = \mathbb{E}_{\Phi_j, |h_k|^2}\left[\prod_{k\in\Phi_j} \exp(-s|h_k|^2\, g(d_k)\mathcal{P}_t)\right].$$

Solving the expectation over $|h_k|^2 \sim \exp(1)$ yields

$$P_{\mathrm{SIR}_j}(d_1, j) = \mathbb{E}_{\Phi_j}\left[\prod_{k\in\Phi_j} \frac{1}{1 + sg(d_k)\mathcal{P}_t}\right].$$

We solve the expectation over the PPP Φ_j using the probability generating functional of the product over PPPs where $\mathbb{E}[\prod_{x\in\Phi_j} f(x)] = \exp[-\alpha_j \int_{\mathbb{R}^2}(1 - f(x))\mathrm{d}x]$, with α_j as the density of Φ_j, converting d_k to polar coordinates, and replacing s, obtaining

$$P_{\mathrm{SIR}_j}(d_1, j) = \exp\left(-2\pi\alpha_j \int_{l_{j-1}}^{l_j} \frac{\delta_{i,j} d_1^\eta}{x^\eta + \delta_{i,j} d_1^\eta} x\, \mathrm{d}x\right). \tag{10}$$

As a contribution over [11], we provide in Appendix VII a closed-form solution for the integral in (10), which we isolate in function $f(\cdot)$. The solution is

$$\begin{aligned} f(d_1, \delta_{i,j}, l_{j-1}, l_j) = {} & \frac{l_j^2}{2}\, {}_2F_1\left(1, \frac{2}{\eta}; 1 + \frac{2}{\eta}; -\frac{l_j^\eta}{d_1^\eta \delta_{i,j}}\right) \\ & - \frac{l_{j-1}^2}{2}\, {}_2F_1\left(1, \frac{2}{\eta}; 1 + \frac{2}{\eta}; -\frac{l_{j-1}^\eta}{d_1^\eta \delta_{i,j}}\right), \end{aligned} \tag{11}$$

and therefore,

$$P_{\mathrm{SIR}_j}(d_1, j) = \exp\left[-2\pi\alpha_j f(d_1, \delta_{i,j}, l_{j-1}, l_j)\right]. \tag{12}$$

Now we consider interference from all SFs when

$$\mathrm{SIR} = \frac{|h_1|^2\, g(d_1)\mathcal{P}_t}{\sum_{j\in S} \mathcal{I}_j}. \tag{13}$$

Following [11], we consider that an outage takes place if the SIR for at least one interfering SF exceeds the threshold in Δ. Conversely, the probability that a collision does not occur is

$$Q_1(d_1) = \prod_{j\in S} P_{\mathrm{SIR}_j}(d_1, j).$$

Since P_{SIR_j}, shown in (12), is an exponential function, we compute the above product by summing the exponents and reorganizing, obtaining

$$Q_1(d_1) = \exp\left(-2\pi \sum_{j\in S} \alpha_j f(d_1, \delta_{i,j}, l_{j-1}, l_j)\right). \tag{14}$$

D. OUTAGE CONDITION 3: EXTERNAL INTERFERENCE

Orfanidis *et al.* [7] report the selectivity of LoRa receivers in the presence of IEEE 802.15.4g signals. We use Orfanidis *et al.* experimentally obtained isolation thresholds to analyze the SIR in the presence of external interference generated by an IEEE 802.15.4g network. Here, we model the IEEE 802.15.4g network as PPP Φ_z and consider [7]

$$\Theta_{[dB]} = \begin{matrix} SF_7 & SF_8 & SF_9 & SF_{10} & SF_{11} & SF_{12} \\ \big[-6 & -9 & -12.5 & -16 & -16 & -16\big], \end{matrix}$$

where Θ denotes the LoRa vs. IEEE 802.15.4g SIR threshold vector, and θ_i denotes the i-th element of Θ, *i.e.*, the SIR threshold for the desired signal in SF ring i and interference from the IEEE 802.15.4g network.

The analysis of the LoRa capture probability in the presence of IEEE 802.15.4g interference is similar to the case for one SF (P_{SIR_j}), but taking the Θ vector and the IEEE 802.15.4g network parameters into account. For

$$\mathrm{SIR}_z = \frac{|h_1|^2\, g(d_1)\mathcal{P}_t}{\sum_{k\in\Phi_z} |h_k|^2\, g(d_k)\mathcal{P}_t}, \tag{15}$$

the *capture probability* w.r.t. external interference is

$$Z_1(d_1) = P_{\mathrm{SIR}_z}(d_1) = \exp(-2\pi\alpha_z f(d_1, \theta_i, 0, R_z)). \tag{16}$$

Note that the model for external interference supports any other communication technology given that adequate SIR thresholds of θ are provided.

V. OPTIMUM LoRaWAN CONFIGURATION

The expressions in Section IV determine the expected reliability of a single node located at a given distance from the gateway. *However, what if one wants to plan the network deployment?* In this section, we consider the use of the previous model to this end. We first consider the inversion of the expressions in the model to obtain network configurations for a targeted minimum average reliability. Afterward, we propose two algorithms that derive optimum network configurations supporting the desired minimum reliability requirement.

A. GUARANTEEING THE RELIABILITY TARGET

To start our search for optimal LoRaWAN configurations we invert the previously described outage expressions defined in (6) and (14), so the network parameters can be extracted from them to achieve a minimum desired reliability level. Note that (16) does not depend on the LoRaWAN configuration. It is, however, taken into account in the optimization algorithm proposed in Sections V-B and V-C to consider external interference. One can assume that, in our network model, the nodes presenting the worst average reliability in each SF ring are those on the outer ring limit. It happens because the signals emitted by those nodes suffer greater path-loss and are, therefore, more susceptible to interference.

1) SF RING LIMITS

As a first step, we find the maximum distance that ensures the required minimum average reliability level w.r.t. the connection probability H_1. We denote this threshold by $\mathcal{T}_{H_1}$. We rewrite (6) to perform operations over the SNR threshold ψ_i in Ψ and the outer SF ring limit l_i,

$$\mathcal{T}_{H_1} = \exp\left(-\frac{\mathcal{N}\psi_i}{\mathcal{P}_t g(l_i)}\right), \tag{17}$$

and then it is straightforward to obtain

$$l_i = \frac{\lambda}{4\pi}\left[-\frac{\mathcal{P}_t \ln(\mathcal{T}_{H_1})}{\mathcal{N}\psi_i}\right]^{\frac{1}{\eta}}. \tag{18}$$

Note that the radius of the overall coverage area is $R = l_6$.

2) RING DENSITIES

Since (18) defines the network geometry, it is now possible to obtain the outage due to external interference observed by the nodes at each ring edge from $Z_1(l_i)$. After that, we compute the maximum densities of the PPPs in Q_1 that satisfy the given final reliability target $\mathcal{T}$, the previously assumed connection reliability target $\mathcal{T}_{H_1}$, and the external interference of each SF i. Thus, following (4), making $C_1(l_i) = \mathcal{T}$ and $H_1(l_i) = \mathcal{T}_{H_1}$, we have for each SF ring i that $\mathcal{T} = \mathcal{T}_{H_1} Q_1(l_i) Z_1(l_i)$, and thus

$$\frac{\mathcal{T}}{\mathcal{T}_{H_1} Z_1(l_i)} = \exp\left(-2\pi \sum_{j\in S} \alpha_j f(l_i, \delta_{i,j}, l_{j-1}, l_j)\right). \tag{19}$$

In (19), the function $f(\cdot)$ is independent of α_j if the SF limits are pre-defined. Then, let $y_{i,j} = f(l_i, \delta_{i,j}, l_{j-1}, l_j)$ and $b_i = -\frac{1}{2\pi}\ln\left(\frac{\mathcal{T}}{\mathcal{T}_{H_1} Z_1(l_i)}\right)$, yielding, for each SF ring i,

$$y_{i,1}\alpha_1 + y_{i,2}\alpha_2 + y_{i,3}\alpha_3 + y_{i,4}\alpha_4 + y_{i,5}\alpha_5 + y_{i,6}\alpha_6 = b_i. \tag{20}$$

If we name the vectors $A = [\alpha_1, \ldots, \alpha_6]$, $B = [b_1, \ldots, b_6]$, and matrix $Y = [y_{i,j}]$, $\forall i, j \in S$, from (20), we derive a system of linear equations $Y \times A = B$ and solve it for the PPPs densities A by making

$$A = Y^{-1} \times B. \tag{21}$$

Note that Y is a $|S| \times |S|$ square matrix, both A and B are row vectors of length $|S|$, and all values $y_{i,j}$ in Y are positive real numbers. To be invertible (Y^{-1}), Y must have a non-zero determinant. Considering the diagonal method to compute the determinant of Y, we observe that, due to Δ, the values at $i = j$ are significantly higher than when $i \neq j$, thus making the positive diagonal greater than the negative diagonal, yielding a determinant that is virtually never zero.

B. MAXIMIZATION OF COMMUNICATION RANGE

The expressions presented above allow us to obtain twelve network parameters: six communication range limits $L = [l_1, \ldots, l_6]$ from (18), and six PPP densities $A = [\alpha_1, \ldots, \alpha_6]$ from (21). Note that (21) depends on (18) because of L. Combining both equations generates an incomplete linear system of six equations and twelve variables. In order to search for optimized feasible network configurations, we propose an algorithm that uses (18) and (21) in an iterative method, trying to extend the outer SF ring limits as much as possible, while preserving the targeted final reliability level $\mathcal{T}$ and ensuring service to a minimum quantity of nodes (N_{min}). The algorithm extends the outer SF ring limits by reducing $\mathcal{T}_{H_1}$. Similarly, increasing $\mathcal{T}_{H_1}$ shortens these limits. The algorithm iteratively guesses values for $\mathcal{T}_{H_1}$ and then, after obtaining L through (18), analyzes the maximum possible densities A. As $\mathcal{T}_{H_1}$ gets closer to $\mathcal{T}$, the capture probability Q_1 increases and, with fixed L and Z_1, higher Q_1 is possible only with lower densities. It may lead to configurations breaking the N_{min} restriction. Conversely, if $\mathcal{T}_{H_1}$ is too close to 1, the outer limits of the SF rings will be shorter, leading to small coverage areas that are useless in practice. However, the proposed algorithm identifies feasible ranges for the network parameters, thus dealing with this parameter trade-off.

Algorithm 1 employs a bisection technique [27] to explore the network design space (*i.e.*, possible values of $\mathcal{T}_{H_1}$), seeking to maximize the width of each SF ring and, as a consequence, the network communication range (disk radius), while preserving the targeted minimum reliability $\mathcal{T}$ and ensuring service to, at least, a given number of nodes (N_{min}). The bisection technique fits well to our problem because it accelerates convergence by reducing the design space in half in each iteration, and it is guaranteed to converge if the problem is feasible. The inputs of the algorithm are the targeted reliability $\mathcal{T}$, the duty-cycle vector p, N_{min}, and the density of IEEE 802.15.4g interfering nodes α_z. The algorithm outputs a *result* variable stating if the algorithm converged (1) or not (-1), the achieved number of nodes N, and the vectors L and A containing, respectively, the rings limits and densities ensuring the target reliability.

After initializing the variables (lines 1-4), the optimization loop starts and runs until the algorithm converges (line 26) or diverges (line 23). The optimization procedure "guesses" values for $\mathcal{T}_{H_1}$, trying to reduce it to enlarge the width of each SF ring, thus increasing the coverage area. Note that since C_1 depends on H_1 from (4), $\mathcal{T}_{H_1}$ must be greater than $\mathcal{T}$;

Algorithm 1 Maximization of SF Rings Widths Given the Target Reliability ($\mathcal{T}$) and the Minimum Number of Nodes (N_{min})

Input: $\mathcal{T}, p, N_{min}, \alpha_z$
Output: result, A, L, N

1: $\mathcal{T}_{H_1,max} \leftarrow 1$
2: $\mathcal{T}_{H_1,min} \leftarrow \mathcal{T}$
3: $R \leftarrow 0, N \leftarrow 0$
4: result $\leftarrow 0$
5: **while** result $= 0$ **do**
6: $\quad \mathcal{T}_{H_1} \leftarrow (\mathcal{T}_{H_1,max} + \mathcal{T}_{H_1,min})/2$
7: $\quad L \leftarrow \frac{\lambda}{4\pi}\left[-\frac{\mathcal{P}_t \ln(\mathcal{T}_{H_1})}{\mathcal{N}\Psi}\right]^{\frac{1}{\eta}}$ {Equation (18)}
8: $\quad R_{last} \leftarrow R$
9: $\quad R \leftarrow L[end]$
10: $\quad R_z \leftarrow R$
11: $\quad$ **for** $i = [1, \ldots, 6]$ **do**
12: $\quad\quad$ **for** $j = [1, \ldots, 6]$ **do**
13: $\quad\quad\quad Y[i,j] \leftarrow f(l_i, \delta_{i,j}, l_j, l_{j+1})$
14: $\quad\quad$ **end for**
15: $\quad\quad B[i] \leftarrow -\frac{1}{2\pi} \ln \frac{\mathcal{T}}{Z_1(l_i)\mathcal{T}_{H_1}}$
16: $\quad$ **end for**
17: $\quad A \leftarrow Y^{-1} \times B$ {Equation (21)}
18: $\quad V \leftarrow$ ComputeRingAreas(L)
19: $\quad N \leftarrow (Ap) \times V'$
20: $\quad$ **if** abs(R - R_{last}) $< \chi$ **and** $A_i \geq 0, \forall A_i$ **then**
21: $\quad\quad$ **if** $N < N_{min}$ **then**
22: $\quad\quad\quad$ **if** $\mathcal{T}_{H_1,max} - \mathcal{T}_{H_1,min} < \epsilon$ **then**
23: $\quad\quad\quad\quad$ result $\leftarrow -1$
24: $\quad\quad\quad$ **end if**
25: $\quad\quad$ **else**
26: $\quad\quad\quad$ result $\leftarrow 1$
27: $\quad\quad$ **end if**
28: $\quad$ **end if**
29: $\quad$ **if** result $= 0$ **then**
30: $\quad\quad$ **if** $A_i \geq 0, \forall A_i$ **and** $N \geq N_{min}$ **then**
31: $\quad\quad\quad \mathcal{T}_{H_1,max} = \mathcal{T}_{H_1}$
32: $\quad\quad$ **else**
33: $\quad\quad\quad \mathcal{T}_{H_1,min} = \mathcal{T}_{H_1}$
34: $\quad\quad$ **end if**
35: $\quad$ **end if**
36: **end while**
37: **return** result, A, L, N

otherwise, both Q_1 and Z_1 would have to be 1, which is impossible in practice. Thus, Algorithm 1 sets the initial search region for $\mathcal{T}_{H_1}$ to $(\mathcal{T}, 1)$. The guessed value for $\mathcal{T}_{H_1}$ in each iteration is at the center of this region, as expressed in line 6. At each iteration, if the selected $\mathcal{T}_{H_1}$ generates a configuration where the number of nodes is above N_{min}, it is assumed that Q_1 can be enhanced by decreasing N, which allows for further decreasing $\mathcal{T}_{H_1}$ in the next iteration. Conversely, if $N < N_{min}$, $\mathcal{T}_{H_1}$ is increased so that Q_1 can be lower, allowing for more nodes in the network. This "binding" part of the algorithm is in lines 30-34.

Provided the branch-and-bound technique guesses $\mathcal{T}_{H_1}$ in line 6, the range limits for all SF are computed using (18) in line 7. In the following, the algorithm uses the newly computed vector L to obtain vector B and matrix Y (lines 11-16), allowing for the computation of the PPPs densities in A (line 17), using (21). Following that, the number of nodes fitting the generated configuration is computed by first obtaining the area of each SF ring in lines 18-19 as $V_i = \pi(l_i^2 - l_{i-1}^2)$. The algorithm converges and stops when the difference in the radius R of the overall coverage area between two consecutive iterations is less than χ (line 20) and $N > N_{min}$ (line 21), where χ defines the precision of R. If the variation of R, *i.e.*, abs($R - R_{last}$), is too small and the algorithm did not achieve N_{min} yet, the algorithm keeps trying to converge until the variation in the guessed $\mathcal{T}_{H_1}$ is below a threshold ϵ (line 22), in which case the algorithm stops and announces a divergence. After evaluating the proposed algorithm for a set of test scenarios, we concluded that good values for the stopping thresholds are $\chi = 1m$ and $\epsilon = 10^{-9}$.

Algorithm 1 always converges if there are feasible solutions to the problem. If the requirements of minimum network density (N_{min} and p), targeted reliability ($\mathcal{T}$), or both, are too high, however, the algorithm may take too long to converge. Hence, we stop the algorithm when the changes in $\mathcal{T}_{H_1}$ get too small (line 22), thus guaranteeing that the algorithm will not run forever since $\mathcal{T}_{H_1,max} - \mathcal{T}_{H_1,min}$ decreases every iteration. It is important to note, however, that achieving higher network density is always possible by reducing the reliability requirement $\mathcal{T}$. Moreover, highly demanding scenarios without feasible solutions or with lengthy convergence are not typical in LoRaWAN, since the technology has been conceived to support massive rather than critical IoT applications.

The algorithm has linear complexity, *i.e.*, $\mathcal{O}(n)$. Analysis of convergence time of this method depends on the precision, which we define in Algorithm 1 as $\chi = 1$ meter. Therefore, the literature defines the maximum number of iterations as $n = \log_2\left(\frac{\chi_0}{\chi}\right)$, where χ_0 is the initial error [27]. In Algorithm 1, $\chi_0 = |R_1 - R_0|$, with $R_0 = 0$ (Algorithm 1, line 3) and R_1 computed in the first iteration (line 9) using (18) with $\mathcal{T}_{H_1} = \frac{1+\mathcal{T}}{2}$ (line 6). Note that although Algorithm 1 involves the solution of a system of linear equations with matrix inversion (line 17) and matrix multiplications (line 19), these are computed quite efficiently since it handles low-dimension matrices – the largest matrix is $\mathbf{Y}$, which is 6-by-6.

C. MAXIMIZATION OF NUMBER OF NODES

Now we consider the case of maximizing the total number of nodes given restrictions of minimum coverage radius (R_{min}) and average reliability ($\mathcal{T}$). We use a more straightforward approach than in Algorithm 1. The problem of maximizing the number of nodes is equivalent to the problem of minimizing Q_1. Thus it is straightforward to conclude, from (4), that we should maximize H_1 because higher H_1 allows for lower Q_1. Since we assume that the worst cases are at the edge of the SFs and we have a restriction on the coverage

Algorithm 2 Maximization of the Number of Nodes Given the Target Reliability ($\mathcal{T}$) and the Minimum Coverage Radius (R_{min})

Input: $\mathcal{T}, p, R_{min}, \alpha_z$
Output: result, A, L, N_{max}
1: $\mathcal{T}_{H_1} \leftarrow \exp\left(-\frac{\mathcal{N}\psi_6}{\mathcal{P}_t g(R_{min})}\right)$
2: $L \leftarrow \frac{\lambda}{4\pi}\left[-\frac{\mathcal{P}_t \ln(\mathcal{T}_{H_1})}{\mathcal{N}\Psi}\right]^{\frac{1}{\eta}}$ {Equation (18)}
3: $R \leftarrow L[end]$
4: $R_z \leftarrow R$
5: **for** $i = [1, \ldots, 6]$ **do**
6: **for** $j = [1, \ldots, 6]$ **do**
7: $Y[i, j] \leftarrow f(l_i, \delta_{i,j}, l_j, l_{j+1})$
8: **end for**
9: $B[i] \leftarrow -\frac{1}{2\pi} \ln \frac{\mathcal{T}}{Z_1(l_i)\mathcal{T}_{H_1}}$
10: **end for**
11: $A \leftarrow Y^{-1} \times B$ {Equation (21)}
12: $V \leftarrow$ ComputeRingAreas(L)
13: $N_{max} \leftarrow (Ap) \times V'$
14: **if** $A_i \geq 0, \forall A_i$ **then**
15: result $\leftarrow 1$
16: **else**
17: result $\leftarrow -1$
18: **end if**
19: **return** result, A, L, N_{max}

radius, the maximum possible H_1 is that yielding $l_6 = R_{min}$. Thus, from (6), we conclude that $\mathcal{T}_{H_1} = H_1(R_{min})$. Assuming the same $\mathcal{T}_{H_1}$ for all SFs, we use (18) to compute L and obtain the geometry of the network.

Once we obtain L, we get the maximum allowable densities ensuring $\mathcal{T}$ through (21) as shown in Algorithm 2. Line 1 uses (6) to compute the maximum $\mathcal{T}_{H_1}$ satisfying R_{min}. Line 2 uses the computed $\mathcal{T}_{H_1}$ to obtain the geometry of the network L. The loop in lines 5-10 computes matrix Y and vector B, so the maximum device density vector A can be computed in line 11. Finally, after computing the areas of the rings and storing them in vector V (line 12), we obtain the maximum number of nodes in line 13.

Note that Algorithm 2 is not iterative since there is no loop searching for the optimum solution and, therefore, it has complexity $\mathcal{O}(1)$. This algorithm merely describes how to use the proposed models to determine the optimum LoRaWAN configuration considering the restrictions. The approach produces unfeasible configurations if the restrictions are too strict. Thus, lines 14-18 check whether the method generated non-negative densities for all SFs to assess whether the results are feasible or not.

VI. NUMERICAL RESULTS

This section evaluates the proposed model and algorithms. In all figures, lines represent theoretical probabilities (*i.e.*, H_1, Q_1, Z_1, Q_1), while marks along the lines show the results of Monte Carlo simulations. Each mark in a figure is the average of 10^5 simulations considering random deployments. Moreover, we assume $F = 6$ dB, $\eta = 2.75$, $\lambda = c/f$ m, $c = 3 \times 10^8$ m/s (speed of light), $f = 868$ MHz for both LoRaWAN and IEEE 802.15.4g . LoRaWAN channel bandwidth is $B_l = 125$ kHz, and IEEE 802.15.4g channel bandwidth is $B_z = 200$ kHz. We also assume that nodes in LoRaWAN and IEEE 802.15.4g transmit with $\mathcal{P}_t = 14$dBm. These parameters configure typical European sub-urban scenarios.

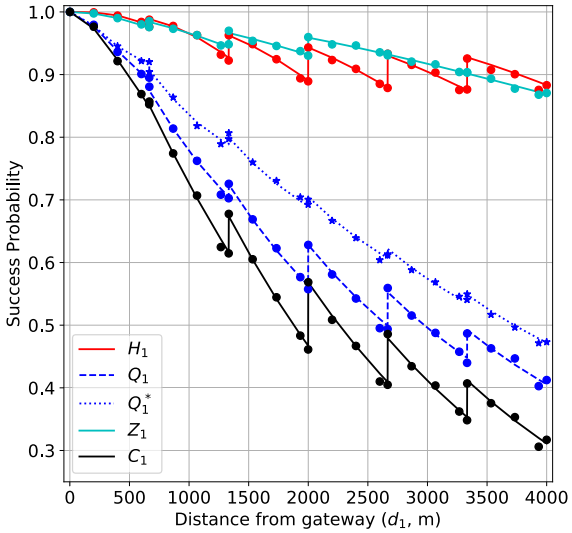

FIGURE 2. Success probabilities of all outage sources. LoRa : $\bar{N} = 4000$, $p = 0.1\%$, $\eta = 2.75$, $\mathcal{P}_t = 14$dBm, $R = 4000m$. IEEE 802.15.4g : $\bar{N}_z = 1000$, $p_z = 0.1\%$, $\eta = 2.75$, $\mathcal{P}_t = 14$dBm, $R_z = 4000m$.

Concerning IEEE 802.15.4g interference, we evaluate the algorithms considering three scenarios. In real deployments, the designer of a LoRaWAN network may not know the operational parameters of the interfering IEEE 802.15.4g network. Thus, in a practical situation, the designer should assume worst-case configurations for the external network.

A. MODEL VALIDATION

Figure 2 aims to validate the presented models by showing the success rates H_1, Q_1, Z_1, and C_1 as a function of the distance from the gateway. The scenario considers an average number of nodes $\bar{N} = 4000$, transmitting with duty cycle $p = 0.1\%$ in a circular area around the gateway with radius $R = 4000$m. The IEEE 802.15.4g network generating external interference has $\bar{N}_z = 1000$ nodes transmitting with duty cycle $p_z = 0.1\%$, also in a circular area with radius $R_z = 4000$m. As can be seen, all theoretical expressions (lines) match the simulation results (marks). One can observe in Z_1 that a relatively light interference from IEEE 802.15.4g ($\bar{N}_z = 1000, p_z = 0.1\%$) has little impact in lower SFs due to the smaller ToA and reduced probability of concurrent transmissions. Higher SFs, on the other hand, have higher ToA and thus suffer more from this external interference.

Also, in Figure 2, Q_1^* shows what the capture probability would be if we consider that LoRa signals are perfectly

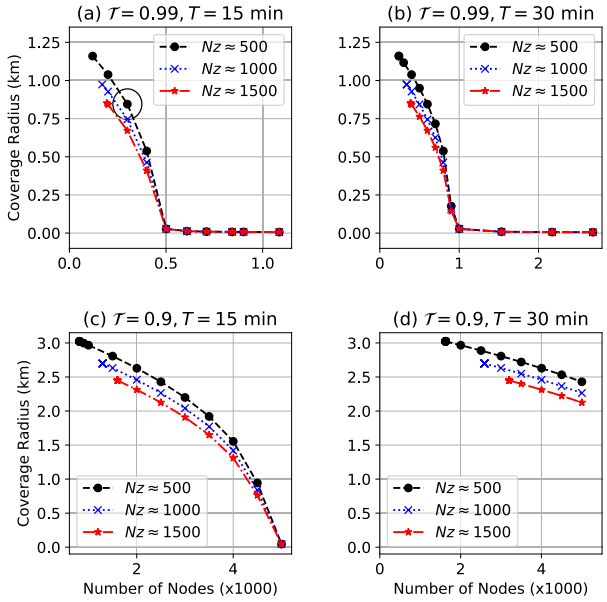

FIGURE 3. Optimization between coverage and number of nodes given a minimum reliability constraint when maximizing R with Algorithm 1.

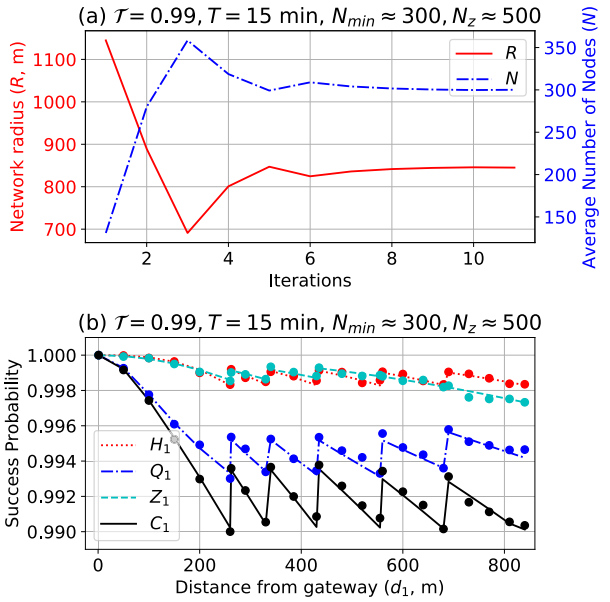

FIGURE 4. Convergence of Algorithm 1 and success probability for the scenario marked in Figure 3a.

orthogonal. We obtain Q_1^* from (14) by considering only $j = i$. As can be seen, the gap between Q_1 and Q_1^* shows that inter-SF interference plays a vital role in link quality.

B. ALGORITHM 1: MAXIMIZATION OF RANGE

Now we evaluate Algorithm 1 of Section V-B. These results use the same network parameters employed to validate the network model. Figure 3 presents a series of graphs for varying optimization objectives. Plots in the same row consider the same reliability target $\mathcal{T}$, while plots in the same column use the same packet generation interval T, expressed in minutes. Each graph shows three curves, each one considering a different amount of IEEE 802.15.4g interference, which varies by changing the number of IEEE 802.15.4g nodes ($\bar{N}_z$), always with duty cycle $p_z = 0.1\%$. Each optimization point considers different N_{min} values, evaluated every 100m.

The first conclusion, when comparing the curves in all plots, is that different IEEE 802.15.4g interference leads to shorter communication ranges when following our proposed optimization procedure. That makes sense since shorter distances feature smaller path loss, making signals less susceptible to external interference. It is also possible to observe that less stringent reliability targets lead to larger coverage areas. Again, that makes sense since smaller $\mathcal{T}$ yields smaller $\mathcal{T}_{H_1}$, which in turn enables longer communication range.

Also, in Figure 3, plot (a) shows the more rigorous scenario; the configuration allowing the required reliability is only practical for $N_{min} \leq 400$ nodes, with a radius varying from 410 to 1160 meters, depending on N_{min} and the external interference. The coverage radius with $N_{min} \geq 500$ either converged to unpractical distances of less than 10 meters or diverged, meaning that we could not place this many LoRaWAN nodes with a packet generation interval of 15 minutes while ensuring minimum reliability of $\mathcal{T} = 0.99$.

For $\mathcal{T} = 0.99$, there are more feasible scenarios if network usage decreases. Plot 3b shows that configurations with up to 900 nodes are possible if the packet transmission interval is $T = 30$ minutes. For $\mathcal{T} = 0.9$ with $T = 15$ minutes, it is possible to find reasonably good network configurations up to $N_{min} = 4500$. However, $N_{min} = 5000$ shrinks the communication range to unpractical distances.

Figure 4 illustrates the behavior of Algorithm 1 and network performance when taking the circled case in Figure 3a as an example. Figure 4a shows the convergence of R and $\bar{N}$ for this scenario. Applying the estimate of the number of iterations presented in Section V-B to this example makes $R_1 = 1244.7$m because of $\mathcal{T} = 0.99$. Therefore, the maximum number of iterations to reach $|R - R_{last}| < \chi$ (line 20, Algorithm 1) is $n = \log_2\left(\frac{\chi_0}{\chi}\right) = \log_2\left(\frac{1244.7}{1}\right) = 10.28$. We see in Figure 4a that the algorithm converges after the 11th iteration with $\bar{N} = 300.1$, thus "stretching" the network range as much as possible. Also, note that convergence time depends on χ_0, which in turn depends on $\mathcal{T}$. If we consider the same case above with $\mathcal{T} = 0.9$ or $\mathcal{T} = 0.8$, we would have, respectively, $\chi_0 = 2899.7$ or $\chi_0 = 3767.3$, what would make, respectively, $n = 11.50$ or $n = 11.88$, showing that the impact of $\mathcal{T}$ in convergence time is small.

Table 2 shows numerical results of the same scenario in two columns: "All sources" with the results for our complete model; and "Intra-SF only" disregarding both inter-SF and external interference sources. We get the results in the "Intra-SF only" column using the same models, but setting $\theta_i = -\infty, \forall i \in S$ in Θ, and $\delta_{i,j} = 1$ for $i = j$ and $\delta_{i,j} = -\infty$ otherwise. When considering all sources of interference,

TABLE 2. Detailed optimization results for the marked scenario in Figure 3a.

Interference:		All sources			Intra-SF only		
Scenario	SF	Range (m)	$\bar{N}_i$	$\bar{N}$	Range (m)	$\bar{N}_i$	$\bar{N}$
3a	7	261.6	162.8	300.1	370.0	124.6	300.0
	8	336.4	67.5		475.7	87.1	
	9	432.4	32.5		611.6	43.5	
	10	555.9	21.8		786.2	25.3	
	11	685.4	10.6		969.3	12.9	
	12	845.0	4.7		1195.1	6.4	

as expected, the fact that ToA impacts the duty cycle induces the optimization procedure to allocate most of the nodes with lower SF. That happens because signal attenuation increases with distance, making more distant nodes more vulnerable to both internal and external interference. Recall that a shorter ToA reduces the collision probability. Moreover, longer ToA generates more internal interference to other SFs.

In some cases, higher SFs may not be used to ensure minimum reliability. However, note that (18), (21), and Algorithm 1 can be extended to change the restriction N_{min} to represent a vector with the minimum number of nodes using each SF. One can achieve that by revisiting the computation of the densities in (21) to consider such a minimum number of nodes when computing the spatial density. Since doing that will possibly result in more nodes using higher SFs, it is expected that fewer nodes use lower SF, resulting in a smaller total number of nodes, as well as a shorter network radius, since the algorithm will converge to a higher H_1 to compensate the increased Q_1. When disregarding inter-SF and external interference, we observe that higher SFs are profoundly affected by inter-SF and external interference, mainly due to their extended ToA. In particular, we observe that interference, rather than path loss, is the main factor for which our method disfavors the use of higher SF. Moreover, it is clear that interference considerably affects coverage.

Finally, Figure 4b shows the success probabilities of the example scenario, where the optimized configurations consider the minimum average reliability target $\mathcal{T}$ for all distances from the gateway. As expected, the success probability approaches the desired minimum $\mathcal{T} = 0.99$ at the edge of each SF. We can see that collisions (Q_1) are kept almost constant or increase slightly with SF. That happens because the algorithm reduces the number of nodes using each SF to keep Q_1 in pace with H_1 and Z_1, to ensure the minimum $\mathcal{T}$.

C. ALGORITHM 2: MAXIMIZATION OF NODES

Now we evaluate Algorithm 2 of Section V-C. The plots in Figure 5 show the results for different scenarios of required minimum reliability ($\mathcal{T}$) and message generation period (T). For all plots, the x-axis represents the R_{min} input to the algorithm, while the y-axis shows the achieved maximized number of nodes. In each plot, the x-axis grows up to the value for which the requirements yield practical results.

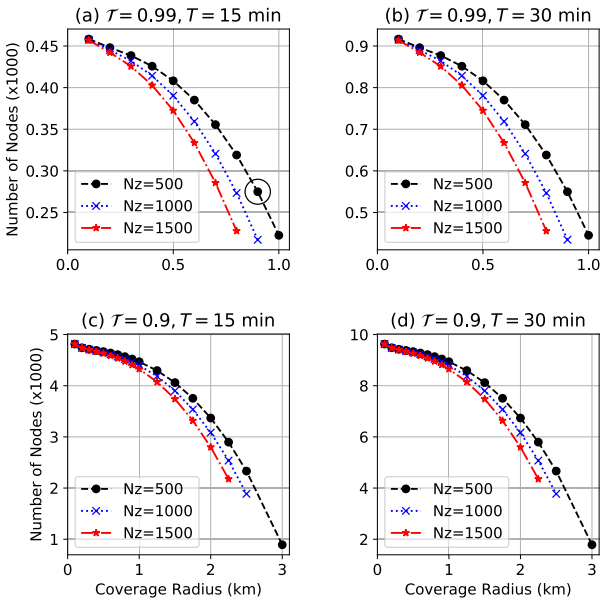

FIGURE 5. Optimization between the number of nodes and coverage given a minimum reliability constraint when maximizing $\bar{N}$ with Algorithm 2.

TABLE 3. Detailed optimization results for the marked scenario in Figure 5a.

Interference:		All sources			Intra-SF only		
Scenario	SF	Range (m)	$\bar{N}_i$	$\bar{N}$	Range (m)	$\bar{N}_i$	$\bar{N}$
5a	7	278.7	149.2	274.9	278.7	211.1	508.2
	8	358.3	61.8		358.3	147.6	
	9	460.6	29.9		460.6	73.7	
	10	592.1	20.2		592.1	42.9	
	11	730.0	9.5		730.0	21.8	
	12	900.0	4.0		900.0	10.9	

In Figure 5, if we analyze each row of plots independently, we see that the maximum number of nodes is a linear function of the transmission period T. For instance, considering $R_{min} = 500$m and $N_z = 500$, N_{max} in plots 5a and 5b are, respectively, 408.18 and 816.36, *i.e.*, N_{max} doubles when T doubles. That is expected since these variations ensure the same network load in all scenarios. We also observe, in all plots, that increased external interference reduces both the number of nodes and the achievable coverage radius.

Table 3 shows the achieved geometry and number of nodes of the marked scenario of Figure 5a. Again, the "All sources" column presents the results of our complete model, while the "Intra-SF only" column disregards inter-SF and external interference. Since the method assumes that the maximum number of nodes is achieved with the shortest possible distances, the maximum range of a node using SF_{12} has to be R_{min} (900m for this case). As for Algorithm 1, Algorithm 2 also favors lower SFs. Moreover, Table 3 shows that the maximum number of nodes almost doubles when disregarding inter-SF and external interference, emphasizing the

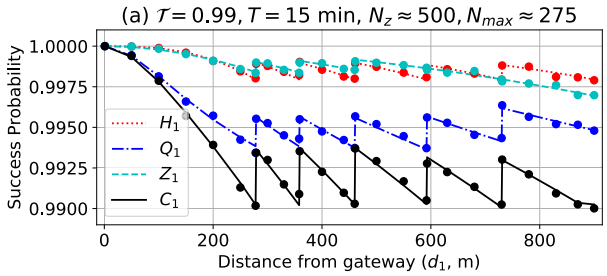

FIGURE 6. Average outage expectation for the marked scenario in Figure 5a.

importance of taking such impairments into account to avoid overestimating the network performance. Finally, Figure 6 shows success probabilities for the example scenario, which approach $\mathcal{T} = 0.99$ at SF edges but stay above the required minimum $\mathcal{T}$ for all distances shorter than R_{min}.

VII. CONCLUSION

This paper presents two algorithms to optimize the configuration of LoRaWAN under imperfect SF orthogonality and IEEE 802.15.4g interference. We use models of LoRaWAN networks to derive success probabilities of packet delivery under internal and external (IEEE 802.15.4g) interference. The presented algorithms search for optimum LoRaWAN configurations given restrictions of minimum network density or coverage radius, meeting a target minimum reliability level. The analytic results are validated using simulations.

Regarding IEEE 802.15.4g interference over LoRaWAN, although higher SF should be more robust to this type of interference, they suffer more from that impairment because their increased ToA makes it more likely that transmissions overlap with IEEE 802.15.4g activity. Finally, regarding the proposed algorithms, they provide a tool for exploring trade-offs between network load and coverage range by showing the feasible region of LoRaWAN network configurations.

Possible future extensions of this work can include other important LPWAN features, such as power allocation and multiple base stations. Moreover, one may consider adapting the proposed algorithms to maximize reliability given fixed network geometry and number of users, in a way similar to what [28] does, or to analyze latency and energy efficiency of the models, similarly to [29], noting that neither [28] nor [29] consider LoRaWAN networks. In the future, we also plan to validate our models using data from a multi-technology large scale IoT network at the University of Oulu.

APPENDIX A: SOLUTION OF $F(D_1, \gamma, L_A, L_B)$

Here we solve the integral in (10). Let

$$f(d_1, \gamma, l_a, l_b) = \int_{l_a}^{l_b} \frac{\gamma d_1^\eta}{x^\eta + \gamma d_1^\eta} x \, \mathrm{d}x.$$

We rearrange $f(\cdot)$ as

$$f(d_1, \gamma, l_a, l_b) = \int_{l_a}^{l_b} x \left(\frac{x^\eta}{d_1^\eta \gamma} + 1 \right)^{-1} \mathrm{d}x$$

and use the binomial theorem $(x+1)^{-1} = \sum_{k=0}^{\infty} (-1)^k x^k$ to obtain

$$f(d_1, \gamma, l_a, l_b) = \int_{l_a}^{l_b} \sum_{k=0}^{\infty} \left(\frac{-1}{d_1^\eta \gamma} \right)^k x^{\eta k + 1} \mathrm{d}x.$$

Since $f(\cdot)$ is continuous in $\mathbb{R}\, \forall x > 0$, we interchange the sum and the integration and solve the integral, yielding

$$f(d_1, \gamma, l_a, l_b) = \sum_{k=0}^{\infty} \left(\frac{-1}{d_1^\eta \gamma} \right)^k \frac{x^{2+\eta k}}{\eta k + 2} \Bigg|_{l_a}^{l_b}.$$

We resort to the Pochhammer function $(a)_k = a(a+1)\cdots(a+k-1) = \frac{\Gamma(a+k)}{\Gamma(a)}$ and to $\frac{(b)_k}{(b+1)_k} = \frac{b}{b+k}$, and reorganize $f(\cdot)$ as

$$f(d_1, \gamma, l_a, l_b) = \frac{x^2}{2} \sum_{k=0}^{\infty} \frac{(1)_k}{k!} \frac{\left(\frac{2}{\eta}\right)_k}{\left(1 + \frac{2}{\eta}\right)_k} \left(-\frac{x^\eta}{d_1^\eta \gamma} \right)^k \Bigg|_{l_a}^{l_b},$$

which is in the form of the Gaussian Hypergeometric function ${}_2F_1(a, b; c; z) = \sum_{k=0}^{\infty} \frac{(a)_k (b)_k}{(c)_k} \frac{z^k}{k!}$ [30], what yields

$$f(d_1, \gamma, l_a, l_b) = \frac{x^2}{2} \, {}_2F_1 \left(1, \frac{2}{\eta}; 1 + \frac{2}{\eta}; -\frac{x^\eta}{d_1^\eta \gamma} \right) \Bigg|_{l_a}^{l_b}.$$

REFERENCES

[1] M. Centenaro, L. Vangelista, A. Zanella, and M. Zorzi, "Long-range communications in unlicensed bands: The rising stars in the IoT and smart city scenarios," *IEEE Wireless Commun.*, vol. 23, no. 5, pp. 60–67, Oct. 2016.
[2] C. Bockelmann, N. Pratas, H. Nikopour, K. Au, T. Svensson, C. Stefanovic, P. Popovski, and A. Dekorsy, "Massive machine-type communications in 5G: Physical and MAC-layer solutions," *IEEE Commun. Mag.*, vol. 54, no. 9, pp. 59–65, Sep. 2016.
[3] (Nov. 2019). *LoRa Alliance*. [Online]. Available: http://www.lora-alliance.org
[4] (Sep. 2019). *Wi-SUN Alliance*. [Online]. Available: http://www.wi-sun.org
[5] K.-H. Chang and B. Mason, "The IEEE 802.15.4g standard for smart metering utility networks," in *Proc. IEEE 3rd Int. Conf. Smart Grid Commun. (SmartGridComm)*, Nov. 2012, pp. 476–480.
[6] L. Zhang, Y. Liang, and M. Xiao, "Spectrum sharing for Internet of Things: A survey," *IEEE Wireless Commun.*, vol. 26, no. 3, pp. 132–139, Jun. 2019.
[7] C. Orfanidis, L. M. Feeney, M. Jacobsson, and P. Gunningberg, "Investigating interference between LoRa and IEEE 802.15.4g networks," in *Proc. IEEE Int. Conf. Wireless Mobile Comput., Netw. Commun. (WiMob)*, Oct. 2017, pp. 1–8.
[8] L. Krupka, L. Vojtech, and M. Neruda, "The issue of LPWAN technology coexistence in IoT environment," in *Proc. 17th Int. Conf. Mechatronics (Mechatronika)*, Dec. 2016, pp. 1–8.
[9] E. De Poorter, J. Hoebeke, M. Strobbe, I. Moerman, S. Latré, M. Weyn, B. Lannoo, and J. Famaey, "Sub-GHz LPWAN network coexistence, management and virtualization: An overview and open research challenges," *Wireless Pers. Commun.*, vol. 95, no. 1, pp. 187–213, 2017.
[10] A. Hoeller, Jr., R. D. Souza, O. L. A. López, H. Alves, M. de Noronha Neto, and G. Brante, "Analysis and performance optimization of LoRa networks with time and antenna diversity," *IEEE Access*, vol. 6, pp. 32820–32829, Jul. 2018.
[11] A. Mahmood, E. G. Sisinni, L. Guntupalli, R. Rondón, S. A. Hassan, and M. Gidlund, "Scalability analysis of a LoRa network under imperfect orthogonality," *IEEE Trans. Ind. Informat.*, vol. 15, no. 3, pp. 1425–1436, Mar. 2019.

[12] R. B. Sørensen, D. M. Kim, J. J. Nielsen, and P. Popovski, "Analysis of latency and MAC-layer performance for class a LoRaWAN," *IEEE Wireless Commun. Lett.*, vol. 6, no. 5, pp. 566–569, Oct. 2017.
[13] O. Georgiou and U. Raza, "Low power wide area network analysis: Can LoRa scale?" *IEEE Wireless Commun. Lett.*, vol. 6, no. 2, pp. 162–165, Apr. 2017.
[14] N. Abramson, "THE ALOHA SYSTEM: Another alternative for computer communications," in *Proc. Fall Joint Comput. Conf.*, Dec. 1970, pp. 281–285.
[15] *AN120.22 LoRa Modulation Basics*, Semtech Corp., Camarillo, CA, USA, Mar. 2015.
[16] *SX1272/73-860 MHz to 1020 MHz Low Power Long Range Transceiver*, Semtech Corp., Camarillo, CA, USA, Mar. 2017.
[17] D. Croce, M. Gucciardo, S. Mangione, G. Santaromita, and I. Tinnirello, "Impact of LoRa imperfect orthogonality: Analysis of link-level performance," *IEEE Commun. Lett.*, vol. 22, no. 4, pp. 796–799, Apr. 2018.
[18] *IEEE Standard for Local and Metropolitan Area Networks—Part 15.4: Low-Rate Wireless Personal Area Networks (LR-WPANs) Amendment 3: Physical Layer (PHY) Specifications for Low-Data-Rate, Wireless, Smart Metering Utility Networks*, IEEE Standard 802.15.4g-2012 Apr. 2012.
[19] M. K. Oh, J. Y. Kim, S. Lee, Y. Jeon, and S. Choi, "A fully integrated IEEE 802.15.4g MR-FSK SoC for smart utility network applications," *IEEE Trans. Consum. Electron.*, vol. 60, no. 4, pp. 580–586, Nov. 2014.
[20] H. Harada, K. Mizutani, J. Fujiwara, K. Mochizuki, K. Obata, and R. Okumura, "IEEE 802.15.4g based Wi-SUN communication systems," *IEICE Trans. Commun.*, vol. E100.B, no. 7, pp. 1032–1043, 2017.
[21] J. Muñoz, T. Chang, X. Vilajosana, and T. Watteyne, "Evaluation of IEEE 802.15.4g for environmental observations," *Sensors*, vol. 18, no. 10, p. 3468, 2018.
[22] *IEEE Standard for Local and Metropolitan Area Networks—Part 15.4: Low-Rate Wireless Personal Area Networks (LR-WPANs) Amendment 1: MAC Sublayer*, IEEE Standard 802.15.4e-2012, Apr. 2012.
[23] U. Deshpande, D. Kotz, and C. McDonald, "Coordinated sampling to improve the efficiency of wireless network monitoring," in *Proc. 15th IEEE Int. Conf. Netw.*, Nov. 2007, pp. 353–358.
[24] M. Haenggi, *Stochastic Geometry Models of Wireless Networks*. Cambridge, U.K.: Cambridge Univ. Press, 2012.
[25] A. Goldsmith, *Wireless Communications*. Cambridge, U.K.: Cambridge Univ. Press, 2005.
[26] C. Goursaud and J.-M. Gorce, "Dedicated networks for IoT: PHY/MAC state of the art and challenges," *EAI Endorsed Trans. Internet-Things*, vol. 15, no. 1, pp. 1–11, Oct. 2015.
[27] R. L. Burden, D. J. Faires, and A. M. Burden, *Numerical Analysis*. Boston, MA, USA: Cengage Learning, 2016.
[28] J. Jia, Y. Deng, J. Chen, A. H. Aghvami, and A. Nallanathan, "Achieving high availability in heterogeneous cellular networks via spectrum aggregation," *IEEE Trans. Veh. Technol.*, vol. 66, no. 11, pp. 10156–10169, Nov. 2017.
[29] A. Mukherjee, "Energy efficiency and delay in 5G ultra-reliable low-latency communications system architectures," *IEEE Netw.*, vol. 32, no. 2, pp. 55–61, Mar. 2018.
[30] A. B. O. Daalhuis, "Hypergeometric function," in *NIST Handbook of Mathematical Functions*, F. W. J. Olver, D. W. Lozier, R. F. Boisvert, and C. W. Clark, Eds., 1st ed. New York, NY, USA: Cambridge Univ. Press, 2010, ch. 15, pp. 383–402.

ARLIONES HOELLER was born in Blumenau, Brazil. He received the B.Sc. and M.Sc. degrees in computer science from the Federal University of Santa Catarina (UFSC), Brazil, in 2004 and 2007, respectively. He is currently pursuing the D.Sc. degree in electrical engineering with the UFSC and the Centre for Wireless Communications (CWC). From 2007 to 2013, he acted as a software engineer and a researcher with Brazilian companies and research institutes, involved in telecommunications and embedded systems projects. Since 2013, he has been a Lecturer with the Federal Institute for Education, Science, and Technology (IFSC), São José, Brazil. Since 2017, he has been a Research Associate with the Circuits and Signal Processing Lab (LINSE), UFSC. Since 2018, he has been a Visiting Researcher with the CWC, University of Oulu, Finland. His current research interests include wireless communications, computer networks, and distributed embedded real-time systems.

RICHARD DEMO SOUZA (S'01–M'04–SM'12) was born in Florianópolis-SC, Brazil. He received the B.Sc. and D.Sc. degrees from the Federal University of Santa Catarina (UFSC), Brazil, in 1999 and 2003, respectively, all in electrical engineering. In 2003, he was a Visiting Researcher with the Department of Electrical and Computer Engineering, University of Delaware, USA. From 2004 to 2016, he was with the Federal University of Technology-Paraná (UTFPR), Brazil. Since 2017, he has been with the Federal University of Santa Catarina (UFSC), Brazil, where he is currently an Associate Professor. His current research interests include wireless communications and signal processing. He is a Senior Member of the Brazilian Telecommunications Society (SBrT). He was a co-recipient of the 2014 IEEE/IFIP Wireless Days Conference Best Paper Award, the Supervisor of the awarded Best PhD Thesis in Electrical Engineering, Brazil, in 2014, and the co-recipient of the 2016 Research Award from the Cuban Academy of Sciences. He has served as an Editor-in-Chief of the SBrT *Journal of Communication and Information Systems*. He served as an Associate Editor for the *IEEE Communications Letters*, the *EURASIP Journal on Wireless Communications and Networking*, and the IEEE TRANSACTIONS ON VEHICULAR TECHNOLOGY.

HIRLEY ALVES received the B.Sc. and M.Sc. degrees from the Federal University of Technology-Paraná (UTFPR), Brazil, in 2010 and 2011, respectively, all in electrical engineering, and the dual D.Sc. degree from the University of Oulu, Oulu, Finland, and UTFPR, in 2015. In 2017, he was an Adjunct Professor in machine-type wireless communications with the Centre for Wireless Communications (CWC), University of Oulu. In 2019, he joined CWC as an Assistant Professor, where he is currently the Head of the Machine-type Wireless Communications Group. His current research interest include massive connectivity and ultra-reliable low latency communications for future wireless networks, 5G and 6G, full-duplex communications, and physical-layer security. He leads the URLLC activities for the 6G Flagship Program. He was a co-recipient of the 2017 IEEE International Symposium on Wireless Communications and Systems (ISWCS) Best Student Paper Award and the 2016 Research Award from the Cuban Academy of Sciences. He has been the organizer, chair, TPC, and tutorial lecturer for several renowned international conferences. He was the General Chair of the ISWCS'2019 and the Co-Chair of the 1st 6G Summit, Levi 2019.

ONEL L. ALCARAZ LÓPEZ was born in Sancti-Spíritus, Cuba, in 1989. He received the B.Sc. degree (Hons.) from the Central University of Las Villas (UCLV), Cuba, in 2013, and the M.Sc. degree from the Federal University of Paraná (UFPR), Brazil, in 2017, all in electrical engineering, with a grant from CAPES/CNPq. He is currently pursuing the Ph.D. degree with the Centre for Wireless Communications (CWC), University of Oulu, Finland. From 2013 to 2015, he was a Specialist in telematics with the Cuban Telecommunications Company (ETECSA). His current research interests include wireless communications, specifically, ultrareliable, low-latency communications for future networks, energy harvesting setups, and efficient access techniques for massive machine-type communications. He is a co-recipient of the 2019 IEEE European Conference on Networks and Communications (EuCNC) Best Student Paper Award and a collaborator to the 2016 Research Award given by the Cuban Academy of Sciences.

SAMUEL MONTEJO-SÁNCHEZ was born in Camagüey, Cuba, in 1979. He received the B.Sc., M.Sc., and D.Sc. degrees from the Central University of Las Villas (UCLV), Cuba, in 2003, 2007, and 2013, respectively, all in telecommunications. From 2003 to 2017, he was an Associate Professor with the Department of Telecommunications, UCLV. In 2011, he was a Visiting Ph.D. Student with the Federal University of Technology-Paraná (UTFPR), Brazil. In 2017, he held a postdoctoral position with the University of Chile. Since 2018, he has been with the Programa Institucional de Fomento a la Investigación, Desarrollo e Innovación (PIDi), Universidad Tecnológica Metropolitana (UTEM), Santiago, Chile. His current research interests include wireless communications, cognitive radio, network coding, energy efficiency, vehicular ad-hoc networks, physical layer security, and the Internet-of-Things. He is a member of the FONDECYT Postdoctoral Grant 3170021, Enabling REsilient urban TRAnsportation systems in smart CiTies (ERANeT LAC) and STIC AnSud (VLmC-Visible Light Mine Communications) projects. He was a co-recipient of the 2016 Research Award from the Cuban Academy of Sciences.

MARCELO EDUARDO PELLENZ was born in Cerro Largo, Brazil, in 1971. He received the B.Sc. degree from the Federal University of Santa Maria, Santa Maria, Brazil, in 1993, and the M.Sc. and D.Sc. degrees from the Department of Communications, State University of Campinas, Campinas, Brazil, in 1996 and 2000, respectively, all in electrical engineering. He is currently a Full Professor with the Pontifical Catholic University of Paraná, Curitiba, Brazil. His current research interests include digital transmission, channel and source coding, wireless networks, wireless sensor networks, network modeling and simulation, and the Internet of Things.